

Simulating the critical behaviour of complex fluids

J. Ilja Siepmann*, Sami Karaborni & Berend Smit†

Shell Research BV, Koninklijke/Shell-Laboratorium, Amsterdam, PO Box 3003, 1003 AA Amsterdam, The Netherlands

ALTHOUGH the liquid–gas phase equilibria of simple fluids have been studied extensively since the seminal work of van der Waals, the properties of fluids with more complex molecular structures, such as polymers, present a less tractable problem both theoretically and experimentally. The phase behaviour of hydrocarbons is of particular importance for the petrochemical industry. But despite significant experimental and theoretical efforts, the phase diagrams of the straight-chain alkanes longer than decane (C_{10}) are known only partially, and even qualitative aspects such as the chain-length dependence of the critical properties are poorly understood. Until recently it was considered impossible to estimate the critical properties of such complex fluids using computer simulations. Here we report Monte Carlo simulations of the phase diagrams of alkanes with unbranched carbon chains as long as C_{48} , up to the vicinity of the liquid–vapour critical points. Our calculations show that, in contrast to the traditional view, the critical density of the long-chain alkanes decreases rather than increases with carbon number. This work indicates that simulations can be used as an ‘engineering tool’ to estimate properties that are not readily accessible experimentally.

Alkanes are thermally unstable above ~ 650 K, which makes experimental determination of the critical points of alkanes longer than decane (C_{10}) extremely difficult, as these tend to lie at still higher temperatures. The longer alkanes, however, are present in mixtures of practical importance for the petrochemical industry. In these mixtures, the number of components can be so large that it is not practical to determine all phase diagrams experimentally. It is therefore necessary to rely on predictions made by equations of state. The parameters of these equations are directly related to the critical properties of the pure components. Therefore, the critical properties of the long-chain alkanes are essential in the design of petrochemical processes, even if they are unstable close to the critical point. Unfortunately, experimental data are scarce and contradictory, and one has to rely on semi-empirical methods to estimate the critical properties¹. Because we can use our simulation technique to study phase behaviour of the longer alkanes at conditions where experiments are not (yet) feasible, we are in a position to make predictions of the critical properties of these molecules.

The simulation technique used here is a combination of the Gibbs-ensemble technique^{2,3} and the configurational-bias Monte Carlo method^{4,5}, the details of which are described in refs 6 and 7. In the Gibbs-ensemble scheme, simulations of the liquid and vapour phases are carried out in parallel. Monte Carlo rules which allow for changes in the number of particles and the volume, ensure that the two boxes (liquid and vapour) are in thermodynamic equilibrium with each other. Because the two boxes are not in ‘physical contact’, there is no interface, and the bulk properties of the two coexisting phases can be obtained directly with a surprisingly small number of particles. This makes the Gibbs ensemble extremely efficient for phase-equilibrium calculations. The major limitation of the Gibbs-ensemble technique is that one of the steps involves the exchange of particles between the two boxes. For liquids consisting of small molecules this does not cause serious problems. For chain molecules, however, the probability of successful exchanges can become very small. For example, under conditions where it takes approximately 10^3 attempts per successful exchange of a methane molecule, it takes

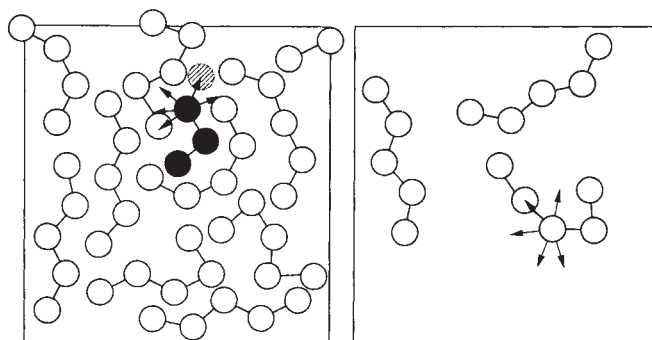


FIG. 1 Schematic drawing of the configurational-bias Monte Carlo algorithm. The figure shows an attempt to exchange a particle from the gas phase (right) into the liquid phase (left). Three segments of the (dark) chain have been grown successfully in the liquid phase and k trial positions are generated (indicated by arrows) to insert the fourth segment. For each of these positions, the energy u_i is calculated and one position is selected (in this case it will be the one with the light shading) with a probability $P_i(l) = \exp(-u_i/k_B T) / W_{\text{new}}(l)$ with $W_{\text{new}}(l) = \sum_{j=1}^k \exp(-u_j/k_B T)$, where T is the temperature and k_B is Boltzmann's constant. This is done for all segments and the factor $W_{\text{new}} = \prod_l W_{\text{new}}(l)$ is determined. For the old configuration $W_{\text{old}} = \prod_l W_{\text{old}}(l)$ is calculated by retracing the ‘path’ of the chain (see diagram of the gas phase, right). For each segment, $k-1$ trial positions are generated which together with the actual position of the segment are used to calculate $W_{\text{old}} = \sum_{j=1}^k \exp(-u_j/k_B T)$. It can be proved that the bias of the insertion can be removed by replacing $\exp(-\Delta U/k_B T)$ in the acceptance rule by $W_{\text{new}}/W_{\text{old}}$ (ref. 6).

of the order of 10^{3n} attempts for a linear alkane with n carbon atoms. The conventional scheme is based on a random insertion of a molecule. In our algorithm, the insertion of the chain is biased. A chain is ‘grown’ atom-by-atom such that regions of favourable energies are found (Fig. 1). The bias is then removed by adjusting the acceptance rules⁶. As a result, the number of successful exchanges is enhanced by an order of magnitude for pentane (C_5) and up to 15 orders of magnitude for octatetracontane (C_{48}).

The Gibbs-ensemble simulations have been performed in cycles. In each cycle a number (equal to the number of particles) of randomly selected Monte Carlo moves are attempted: displacements of a molecule, rotation of a molecule, volume change

TABLE 1 Details of the n -alkanes model

Physical aspect	Potential function	Parameters
Non-bonded interactions	$U_{\text{L}}(r_{ij}) = 4\epsilon_{ij}((\sigma_{ij}/r_{ij})^{12} - (\sigma_{ij}/r_{ij})^6)$	$\sigma_{\text{CH}_3} = \sigma_{\text{CH}_2} = 3.93 \text{ \AA}$ $\epsilon_{\text{CH}_3} = 114.0 \text{ K}$ $\epsilon_{\text{CH}_2} = 47.0 \text{ K}$
Bond-bending	$U_{\text{bending}}(\theta_i) = 1/2 K_{\theta}(\theta_i - \theta_{\text{eq}})^2$	$k_{\theta} = 62,500 \text{ K rad}^{-2}$ $\theta_{\text{eq}} = 114^\circ$
Angle torsion	$U_{\text{torsion}}(\phi_i) = a_1(1 + \cos \phi_i) + a_2(1 - \cos(2\phi_i)) + a_3(1 + \cos(3\phi_i))$	$a_1 = 355.03 \text{ K}$ $a_2 = -68.19 \text{ K}$ $a_3 = 791.32 \text{ K}$

The model is based on the united-atom description, that is methyl or methylene groups are considered as single interaction centres. The pseudo-atoms in a given chain are assumed to be connected by rigid bonds ($d_{\text{CC}} = 1.54 \text{ \AA}$). The non-bonded interactions are described by Lennard–Jones potentials which are truncated at 13.8 \AA . The usual tail corrections¹⁵ are used to estimate the interactions beyond the cut-off. The parameters for the unlike interactions have been calculated using $\epsilon_{ij} = \sqrt{\epsilon_i \epsilon_j}$. Bond-bending is modelled by a harmonic potential¹⁶ and changes in the torsional angles are controlled by the Jorgenson potential¹¹.

* Present address: Department of Chemistry, University of Pennsylvania, Philadelphia, Pennsylvania 19104-6323, USA.

† To whom correspondence should be addressed.

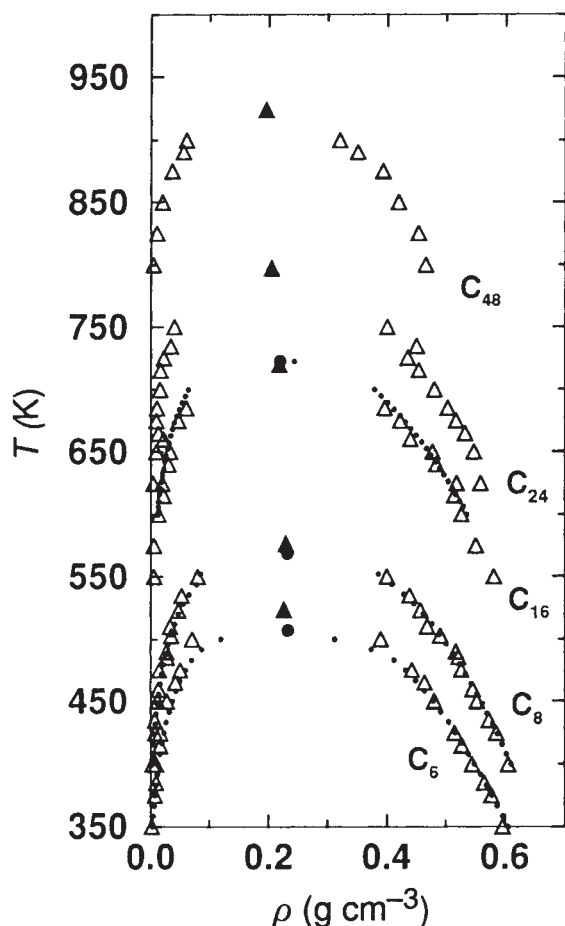


FIG. 2 The vapour-liquid curves of various alkanes, plotted as temperature T against density ρ . Simulations are represented by open triangles and the critical point by a large filled triangle. The experimental results are represented by black dots (C_6 , C_8 are from ref. 17 and the data for C_{16} are estimates from an equation of state). The experimental critical points (represented by large filled circles) are from ref. 14. The simulations were performed with numbers of molecules ranging from 200 (for C_5), to 100 (for C_{48}); the number of trial orientations in the configurational-bias Monte Carlo scheme range from 5 (for C_5) to 10 (for C_{48}). The number of equilibrium cycles was at least 3,000 for C_5 ranging to 6,000 for C_{48} , and production runs were performed over at least 5,000 cycles for all molecules.

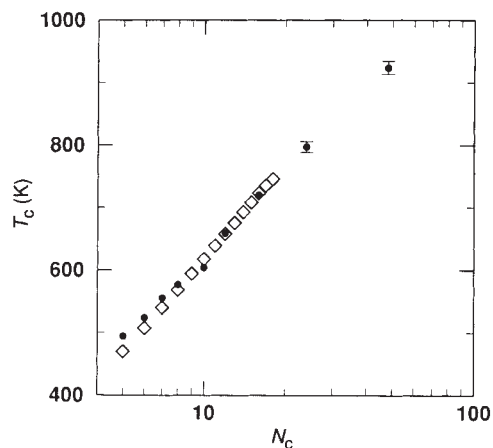


FIG. 3 Critical temperature of the normal alkanes (T_c) as a function of the carbon number (N_c). The experimental data of Anselme *et al.*¹⁴ and Steele¹³ are represented by squares and the results from the simulations by filled circles. Error bars are shown when larger than the symbol size.

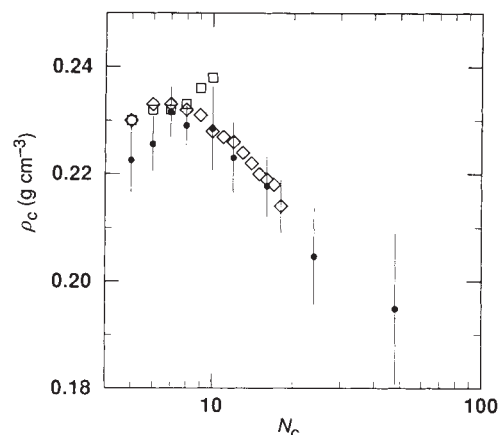


FIG. 4 Critical density of the normal alkanes (ρ_c) as a function of the carbon number (N_c). The experimental data of Anselme *et al.*¹⁴ are represented by diamonds, the data of Steele¹³ by squares and the results from the simulations by filled circles. Note that for C_5 the data of Anselme *et al.* and Steele coincide.

of the two boxes, re-growing parts of a molecule, and exchanging molecules between the two boxes. For the latter two moves configurational-bias Monte Carlo has been used. For systems with strong intramolecular interactions it is important to take these interactions into account when generating the trial orientations in the configurational-bias Monte Carlo scheme^{5,8}. The probability of acceptance of an exchange move ranged from 2–10% for C_5 to 0.5–3% for C_{48} , depending on the temperature. The results of the Gibbs-ensemble simulations are analysed using the techniques described in ref. 9 and the critical point is estimated using the procedure given in ref. 10.

Phase diagrams are very sensitive to the choice of interaction potentials. Most available models for alkanes have been obtained by fitting simulation data to experimental properties of the liquid at standard conditions. We have tested several of the published alkane models, but it turned out that none of them was able to reproduce the liquid-vapour coexistence properties for both short and long chains. For instance, the models of refs 11 and 12 give nearly identical liquid properties in standard conditions, but yield estimates of the critical temperature of octane that differ by 100 K. For this reason, we developed a new set of energy and size parameters of the intermolecular potential, the intramolecular potentials being taken directly from the literature. Details of the potentials are given in Table 1. The coexistence curves, shown in Fig. 2, demonstrate that our model is in satisfactory agreement with the experimental data.

In Fig. 3 the critical temperature is plotted against the carbon number. The simulations reproduce the experimental critical temperatures very well. There is, however, considerable disagreement between the various experimental estimates of the critical densities. Much of our current knowledge of the critical properties of the higher alkanes is based on extrapolations of fits to the experimental data up to C_8 . The most widely used extrapolations assume that the critical density is a monotonically increasing function of the carbon number, approaching a limiting value for the very long alkanes^{1,13}. In contrast to such predictions based on extrapolation, recent experimental data¹⁴ indicate that the critical density reaches a maximum at C_8 and then decreases monotonically. Other data¹³, however, do not give any evidence for such a maximum (Fig. 4). Our simulations indicate the same trend as that observed by Anselme *et al.*¹⁴. Because calculations can also be done for much longer alkanes, our results strongly support the latter experiments.

Our work shows that simple group-contribution like intermolecular potentials can be developed to model systems of

industrial importance accurately. Simulations could therefore become an important technique for estimating properties of systems that are difficult to study by traditional methods. The techniques employed here are not limited to *n*-alkanes but can be applied in many other computer simulations of complex fluids. □

Received 15 June; accepted 9 August 1993.

1. Tsouropoulos, C. *A.I.Ch.E. J.* **33**, 2080–2083 (1987).
2. Panagiotopoulos, A. Z. *Molec. Phys.* **61**, 813–826 (1987).
3. Panagiotopoulos, A. Z., Quirk, N., Stapleton, M. & Tildesley, D. J. *molec. Phys.* **63**, 527–545 (1988).
4. Siepmann, J. I. & Frenkel, D. *Molec. Phys.* **75**, 59–70 (1992).
5. Frenkel, D., Mooij, G. C. A. M. & Smit, B. J. *Phys.: Condensed Matter* **4**, 3053–3076 (1992).

6. Mooij, G. C. A. M., Frenkel, D. & Smit, B. J. *Phys.: Condensed Matter* **4**, L255–L259 (1992).
7. Laso, M., de Pablo, J. J. & Suter, U. W. J. *chem. Phys.* **97**, 2817–2819 (1992).
8. Siepmann, J. I. & McDonald, I. R. *Molec. Phys.* **79**, 457–473 (1993).
9. Smit, B., de Smedt, Ph. & Frenkel, D. *Molec. Phys.* **68**, 931–950 (1989).
10. Smit, B. & Williams, C. P. J. *Phys.: Condensed Matter* **2**, 4281–4288 (1990).
11. Jorgensen, W. L., Madura, J. D. & Swenson, C. J. *J. Am. chem. Soc.* **106**, 6638–6646 (1984).
12. Toxvaerd, S. J. *chem. Phys.* **93**, 4290–4295 (1990).
13. Tsouropoulos, C. & Tan, Z. *Fluid Phase Equilibria* **83**, 127–138 (1993).
14. Anselme, M. J., Gude, M. & Teja, A. S. *Fluid Phase Equilibria* **57**, 317–326 (1990).
15. Allen, M. P. & Tildesley, D. J. *Computer Simulation of Liquids* (Clarendon, Oxford, 1987).
16. Van der Ploeg, P. & Berendsen, H. J. C. *J. chem. Phys.* **76**, 3271–3276 (1982).
17. Smith, B. D. & Srivastava, R. *Thermodynamics Data for Pure Compounds: Hydrocarbons and Ketones* (Elsevier, Amsterdam, 1986).

ACKNOWLEDGEMENTS. We thank M. J. Anselme, D. Frenkel, W. G. Heitman, A. K. van Helden, H. P. C. E. Kuipers and S. Schreuder for comments.

The influence of water on the petrogenesis of subduction-related igneous rocks

Glenn A. Gaetani*, Timothy L. Grove* & Wilfred B. Bryan†

* Department of Earth, Atmospheric and Planetary Sciences, Massachusetts Institute of Technology, Cambridge, Massachusetts 02139, USA

† Woods Hole Oceanographic Institute, Woods Hole, Massachusetts 02543, USA

THE presence of dissolved water can significantly change the sequence in which different minerals crystallize from a silicate magma^{1,3}. This will alter the compositional path followed by residual liquids (the 'liquid line of descent'), and modify the types and compositions of crystals that accumulate at the site of cooling. The sharp decrease in the solubility of water in silicate melts with decreasing pressure makes direct measurements of pre-eruptive concentrations in magmas difficult because much of the dissolved water boils off before eruption. Here we report experimental results on the crystallization of basalts that contain substantial dissolved water (up to 6 wt%), and show how the results can be used to infer the amount of dissolved H₂O involved in the petrogenesis of lavas that preserve a record of their liquid lines of descent, or the accumulated minerals left behind after solidification. The presence of abundant magmatic water is a signature of subduction-zone volcanism⁴, and can be used to associate a suite of magmas or igneous cumulates with a convergent-margin, back-arc or inter-arc tectonic setting.

Compositional variations observed in spatially and temporally associated volcanic rocks have traditionally been interpreted as a record of the conditions in which the parent magma crystallized. Similarly, the mineral associations and the compositional variations in the accumulated crystals preserve a record of the conditions of solidification. (Other magmatic processes that can lead to compositional variations in arc magmas include magma mixing and assimilation of crust and mantle. The influence of these other processes can be recognized and must be accounted for along with the effects of crystal fractionation.) The compositional variations in suites of island-arc basalts are often consistent with the early crystallization of olivine + clinopyroxene⁵, whereas the systematics of mid-ocean-ridge basalt suites point to olivine + plagioclase as the early crystallizing phases⁶. Olivine and high-Ca clinopyroxene are found together in igneous ultramafic cumulate rocks (wehrlites and olivine clinopyroxenites), and this association has been interpreted as an indication of crystallization at elevated pressure in the upper mantle^{7,8}. We use new experimental results (see ref. 9 for details) to show that

the signature of early olivine + high-Ca pyroxene crystallization in island-arc basalts results from magmatic H₂O contents of ~2–4 wt% at crustal pressures (6–10 km depth). We also show that the cumulates left behind by hydrous, low-pressure crystallization processes are distinct from those formed under anhydrous conditions at elevated pressures.

Melting experiments have established that primitive, sub-alkaline lavas, including both mid-ocean-ridge and high-alumina basalts, crystallize olivine ± plagioclase at crustal pressures under anhydrous conditions^{10,12}; clinopyroxene crystallizes in relatively evolved lavas. This crystallization sequence will accordingly produce olivine (dunite), olivine + plagioclase (troctolite) and olivine + plagioclase + clinopyroxene (olivine gabbro) cumulates. A few experimental studies have found olivine + clinopyroxene near the anhydrous liquidus at high pressures (~8–10 kbar)^{8,13,14}, leading to the common assumption that olivine + clinopyroxene cumulates form by crystallization in upper-mantle conditions.

Water-saturated melting experiments performed on an (olivine + high-Ca clinopyroxene)-bearing basalt from ODP Leg 135 Hole 839B, in the Lau basin, produced an extended interval of olivine + clinopyroxene crystallization at a pressure of only 2 kbar (~6 km depth). This basalt was chosen for experimental study because it is fine-grained, equigranular and lacks complex phenocrysts. It therefore represents a liquid composition. This basalt crystallizes olivine + plagioclase near its liquidus at 1 atm,

TABLE 1 Electron microprobe analyses of experimental run products and xenolith clinopyroxenes

	1	2	3	4	5	6
SiO ₂	53.3 (2)	53.5 (1)	54.4 (1)	52.4 (4)	51.94	51.1
TiO ₂	0.60 (3)	0.73 (3)	0.70 (5)	0.33 (9)	0.36	0.48
Al ₂ O ₃	15.16 (8)	14.26 (7)	17.7 (1)	2.9 (3)	2.55	7.5
Cr ₂ O ₃	0.05 (3)	0.07 (3)	0.03 (2)	0.6 (1)	0.10	1.4
FeO*	8.85 (8)	9.4 (1)	8.0 (1)	6.4 (9)	4.12	4.9
MnO	0.22 (2)	0.19 (3)	0.22 (4)	0.18 (3)	0.21	—
MgO	9.36 (5)	7.91 (9)	5.85 (6)	16.9 (5)	16.22	17.9
CaO	11.3 (1)	11.5 (2)	10.8 (1)	20.5 (7)	24.82	14.4
Na ₂ O	1.48 (5)	1.55 (6)	1.85 (9)	0.14 (2)	0.20	1.0
K ₂ O	0.30 (2)	0.30 (1)	0.34 (1)	—	—	0.11
P ₂ O ₅	0.11 (3)	0.16 (2)	0.20 (3)	—	—	—
Total	100.73	99.57	100.09	100.35	100.52	98.79

Analyses given in wt%. 1. Sample 135–839B-15R-2, 63–67 cm melted at 1,210 °C, 1 atm⁹; 2. glass from sample 135–839B-15R-2, 63–67 cm after 18% crystallization at 1 atm under anhydrous conditions⁹; 3. glass from sample 135–839B-15R-2, 63–67 cm after 17% crystallization at 2 kbar under H₂O-saturated conditions⁹; 4. clinopyroxene coexisting with glass no. 3 from 2 kbar, H₂O-saturated melting experiment⁹; 5. clinopyroxene from low-pressure wehrlite xenolith from Adak island, Aleutian arc³¹; 6. clinopyroxene from high-pressure wehrlite xenolith from Black Rock Summit, Nevada, USA³². (Units in parentheses represent one standard deviation of least units cited, based on replicate analyses. Therefore, 53.3(2) should be read 53.3 ± 0.2.)